

Characterization of Tungsten-Based Pillars Deposited by Helium Ion Microscope Equipped with Gas Injection System

Kazuyuki Kohama^{1,4}, Tomohiko Iijima², Misa Hayashida³, Shinichi Ogawa¹

¹Nanoelectronics Research Institute, National Institute of Advanced Industrial Science and Technology (AIST), 16-1, Onogawa, Tsukuba, 305-8569 Ibaraki, Japan

Phone: +81-29-860-5091 E-mail: kazuyuki-kohama@aist.go.jp

²Innovation Center for Advanced Nanodevices, AIST, 16-1, Onogawa, Tsukuba, 305-8569 Ibaraki, Japan

³National Metrology Institute of Japan, AIST, 1-1-1, Higashi, Tsukuba, 305-8565 Ibaraki, Japan

⁴Research Fellow of the Japan Society for the Promotion of Science

1. Introduction

In order to achieve a higher integration density in semiconductor devices, development of three-dimensional (3D) integration methods such as vertical chip-to-chip bonding using conductive metal pillars and dots is needed. We recently applied a helium ion microscope (HIM) equipped with a tungsten hexacarbonyl ($W(CO)_6$) gas injection system (GIS) to formation of tungsten-based dot markers on a transmission electron microscope (TEM) tomography sample for a precise three dimensional observation by helium ion beam-induced deposition [1]. Comparing with a conventional focused ion beam (FIB) system with a gallium ion source, the HIM-GIS method could form much smaller tungsten dots of a few nm due to its smaller beam diameter (~ 0.25 nm at 0.1 pA and ~ 2 nm at 1.0 pA) [2] and lower secondary electron (SE) energy (~ 1 eV) [3]. Those properties might realize formation of finer pillars with moderate gas reactions, contrary to severe reactions induced by higher energy SEs in conventional electron beam microscopy or Ga FIB. Thus, tungsten-based pillars with a high aspect ratio are expected to be formed by the HIM-GIS method, which is attractive for the 3D structure, MEMS, sensor, and other applications. In this study, we demonstrated the formation of tungsten-based pillars by the HIM-GIS method, and then characterization of the pillars was carried out for fundamental investigation.

2. Experimental Procedures

The HIM-GIS system with $W(CO)_6$ gaseous precursor was used for the deposition of the tungsten-based pillars. The pillars were deposited on four types of target materials such as amorphous carbon, Si(100) wafer with native oxide, 400 nm-thick SiO_2 layer grown on Si, and tungsten film. The helium ion beam energy (30 keV) and the precursor source condition were fixed during the deposition. The beam current, working distance (WD) and deposition duration varied in the range between 0.2 - 1.0 pA, 10.3 - 12.0 mm and 5 - 240 s, respectively. The WD is the distance between the objective lens and the target, and can be controlled by changing the target height position. Note that the position of the precursor gas injection nozzle was fixed below the lens, thus the nozzle - target distance varied with the WD. The tungsten-based pillars were observed and characterized by HIM SE imaging mode, TEM, and scanning TEM (STEM).

3. Results and Discussion

Figure 1(a) shows a TEM bright-field image of five tungsten pillars sequentially deposited on the amorphous carbon target under the same condition as follows: the beam current and WD were kept at 0.9 pA and 10.5 mm, respectively, and the deposition duration was set for 120 s. The continuous tungsten-based pillars with an aspect

ratio of ~ 50 were successfully formed by the HIM-GIS method. The width and height of the pillars were ~ 40 nm and ~ 2 μ m, respectively. It is not clear why the pillar width (~ 40 nm) was much thicker than the incident beam diameter ($< \sim 2$ nm), however, the reason may be correlated to scattering of the helium ion beam and the SE generation mechanism at growing surface. Figure 1(b) shows a diffraction pattern taken from the five tungsten pillars shown in Fig. 1(a). The diffraction spots were in good agreement with a diffraction-ring pattern of a face-centered cubic (FCC) structure, and the lattice constant was estimated to be 0.42 nm. Considering both of the crystal structure and the lattice constant, the pillars consisted of WC_{1-x} or $W_2(C, O)$ grains, rather than body-centered-cubic tungsten grains.

Figure 2(a)-2(d) show STEM bright-field image of the tungsten-based pillars deposited on the four types of target materials with the beam current and WD of 1.0 pA and 10.5 mm, respectively. The pillar size and shape were found to be similar for all the target materials. An example of high-resolution lattice images taken in the pillars and its Fourier transformation pattern are shown in Fig. 2(d') and 2(d''), respectively. The pattern was in good agreement with the pattern of the FCC structure with the lattice constant of 0.42 nm. Similarly, the FCC crystalline grains were identified in all the other samples, and thus selection of target materials would not have significant influence on the pillar growth and crystal structure.

In order to investigate effects of the beam current and WD on the vertical growth rate, tungsten-based pillars were deposited on the Si target. Figure 3 shows the vertical growth rate plotted as a function of the WD. The current difference is indicated by different symbols. The growth rate decreased with increasing the WD, indicating the precursor gas flux at the deposition site decreased with the WD. Although the growth rates for the pillars deposited with the WD of 10.3 mm were widely distributed depending on the beam current, those with the WD of 11.0 mm were similar regardless of the beam current. This suggests that depletion of the precursor gas occurred at the deposition site when the deposition was performed with higher beam current and larger WD.

To clarify the effects of the precursor gas flux at the deposition site on the microstructure of the tungsten-based pillars, STEM observation was performed. Figure 4(a) shows a high-angle annular dark field (HAADF) image of the pillar deposited on the SiO_2 target with the beam current and WD of 1.0 pA and 10.5 mm, respectively. As shown in Fig. 4(a), uniform white contrast was observed, indicating the pillar was formed continuously and homogeneously. On the contrary, a columnar void was observed in the pillar deposited with the WD of 11.5 mm, as shown in Fig. 4(b). Similarly, an STEM top view of a tungsten dot deposited on the amorphous carbon target with

the beam current and WD of 1.0 pA and 12.0 mm, respectively, shows a void surrounded by the FCC lattice pattern (Fig. 5). The position of the void presumably corresponds to the beam irradiation point, where the pillar might be sputter etched by the incident beam continuously. The larger WD would cause depletion of the precursor gas at the deposition site, and thus the sputter etch by the helium ion beam might be enhanced. These results lead to a conclusion that formation of the tungsten-based pillars is controlled by a balance between the beam-induced deposition and sputter etch, thus the beam current and the precursor gas flux play important roles for fabrication of continuous tungsten-based pillars with high aspect ratio.

4. Conclusions

The tungsten-based pillars composed of FCC- $W_{1-x}O_x$ or $W_2(C, O)$ grains with aspect ratio of ~ 50 were formed by the HIM-GIS method. Difference of target materials would not have significant influence on the pillar growth and crystal structure. On the other hand, the columnar void was formed in the middle of the pillar when the

deposition was performed with the high beam current and large WD, indicating the formation of the tungsten-based pillars is controlled by a balance between the beam-induced deposition and sputter etch. The beam current and the precursor gas flux play important roles for fabrication of continuous tungsten-based pillars with high aspect ratio.

Acknowledgements

Authors thank M. Tsukahara and K. Shinoda for their help in the STEM work, and H. Akinaga for his encouragement throughout this work. This work was supported by Research Fellowships of the Japan Society for the Promotion of Science for Young Scientists (Kohama).

References

- [1] M. Hayashida et al., *Micron*, **43** (2012) 992.
- [2] S. Ogawa, in private communications.
- [3] Y. V. Petrov et al., *J. Surface Investigation*, **4** (2010) 792.

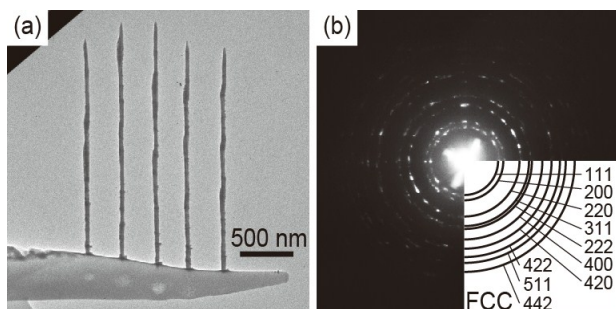


Fig. 1 (a) A TEM bright-field image of the five tungsten pillars sequentially deposited on the rod-shaped amorphous carbon target with the beam current, WD and deposition duration of 0.9 pA, 10.5 mm and 120 s, respectively. (b) A diffraction pattern taken from the five tungsten pillars shown in (a).

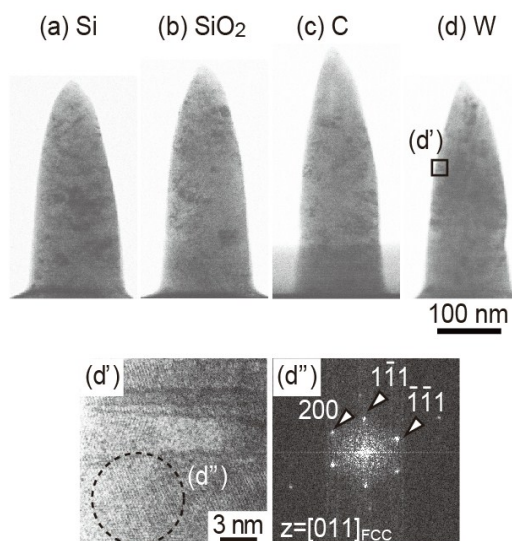


Fig. 2 STEM bright-field images of the tungsten-based pillars deposited on the (a) Si, (b) SiO_2 , (c) carbon and (d) tungsten targets with the beam current, WD and deposition duration of 1.0 pA, 10.5 mm and 60 s, respectively. (d') A high-resolution lattice image taken in the area marked with a square in (d). (d'') A Fourier transformation pattern created from the area marked with a broken circle in (d')

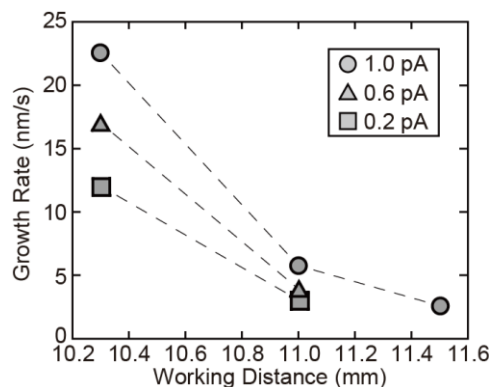


Fig. 3 The vertical growth rate of the tungsten-based pillars plotted as a function of the WD.

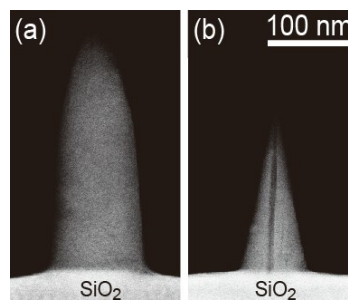


Fig. 4 HAADF-STEM images of the tungsten-based pillars deposited on the SiO_2 target with the WD of (a) 10.5 mm, (b) 11.5 mm. The beam current and deposition duration were 1.0 pA and 60 s, respectively.

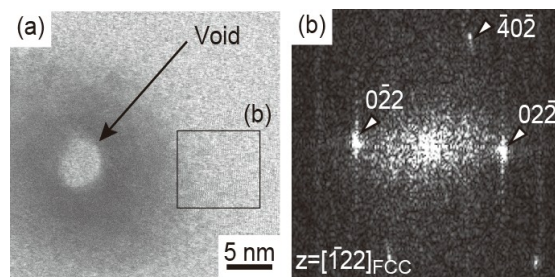


Fig. 5 (a) An STEM top view of the tungsten dot deposited on the amorphous carbon target with the beam current, WD and deposition duration of 1.0 pA, 12.0 mm and 5 s, respectively. (b) A Fourier transformation pattern created from the area marked with a square in (a).